KAONNIS

L. Abbene (Assoc.), F. Artibani (Dott.), M. Bazzi,
D. Bosnar (Assoc.), A. Buttacavoli (Assoc.), A. Clozza, F. Clozza (Dott.),
C. Curceanu (Resp. Naz.), R. Del Grande (Ric. Str.), L. De Paolis (Assegn.),
P. Levi Sandri, M. Iliescu, S. Manti (Assegn.), C. Milardi, M. Merafina (Assoc.),
F. Napolitano (Assoc.), E. Pace, F. Principato (Assoc.), A. Scordo,
F. Sgaramella (Dott.), D. Sirghi (Assoc.), F. Sirghi, M. Skurzok (Assoc.),
A. Spallone (Assoc.), K. Toho (Dott.), O.Vazquez Doce

1 KAONNIS: the scientific program

KAONNIS represents an integrated initiative in experimental low-energy kaon-nucleon/nuclei interaction studies. Under KAONNIS the following activities are performed:

- kaonic atoms measurements by the SIDDHARTA-2 experiment
- studies of kaon-nuclei interactions at low-energies in the framework of the AMADEUS Collaboration
- participation at experiments at J-PARC (Japan) dedicated to strangeness studies
- future kaonic atoms measurements program at the DAΦNE collider or/and J-PARC.

We present in what follows the KAONNIS 2025 activities and plans for 2026.

2 The SIDDHARTA-2 experiment

The objective of the SIDDHARTA-2 (Silicon Drift Detector for Hadronic Atom Research by Timing Application) experiment is to perform high precision measurements of X-ray transitions in exotic (kaonic) atoms at the DAΦNE collider.

The precise measurement of the shift and width of the 1s level, with respect to the purely electromagnetic calculated values, in kaonic hydrogen and kaonic deuterium, induced by the strong interaction, through the measurement of the X-ray transitions to this level, will deliver the first precise experimental determination of the isospin-dependent antikaon-nucleon scattering lengths, fundamental quantities for the understanding of the strong interaction in strangeness sector.

The accurate determination of the scattering lengths will place strong constraints on the low-energy K^- N dynamics, which, in turn, constraints the SU(3) description of chiral symmetry breaking in systems containing the strange quark. The implications extend from particle and nuclear physics to astrophysics (the equation of state of neutron stars).

The SIDDHARTA collaboration performed the most precise measurement of kaonic hydrogen and the first exploratory study of kaonic deuterium. Moreover, the kaonic helium 4 and 3 transitions to the 2p level were measured, for the first time in gas in He^4 and for the first time ever in He^3.

The SIDDHARTA-2 experiment successfully completed its kaonic deuterium run in June 2024, collecting more than 800 pb^{-1} of data, which are under analysis. It has also performed a series of other measurements, including the most precise determination of the KHe-4 L_α, transition and yields in gas, the first observation of the KHe-4 M-series transitions, a precision measurement of the high-n transitions in kaonic carbon, oxygen, nitrogen and aluminium and a measurement of kaonic neon transitions.

2.1 The SIDDHARTA experiment

In the first decade of this century, SIDDHARTA represented a new phase in the study of kaonic atoms at DAΦNE. The previous DEAR experiment's precision was limited by a signal/background ratio of about 1/70 for the kaonic hydrogen measurement, due to the high machine background. To significantly improve this ratio, an experimental breakthrough was necessary. An accurate study of the background sources at DAΦNE was done. The background includes two main sources:

- *synchronous background*: coming from the K^- interactions in the setup materials and Φ-decay processes; it can be defined as *hadronic background*;
- *asynchronous background*: final products of electromagnetic showers in the machine beam pipe and in the setup materials, originating from particles lost from primary circulating beams either due to the interaction of particles in the same bunch (Touschek effect) or due to the interaction with the residual gas.

Accurate studies showed that the main background source in DAΦNE is of the second type, which points to the procedure to reduce it. A fast trigger correlated to the kaons entering into the target cuts the main part of the asynchronous background. X rays were detected by DEAR using CCDs (Charge-Coupled Devices), which are excellent X-ray detectors, with very good energy resolution (about 140 eV FWHM at 6 keV), but having the drawback of being non-triggerable devices (since the read-out time per device is at the level of 10 s). A new device, which preserves all good features of CCDs (energy resolution, stability and linearity), but additionally is triggerable - i.e. fast (at the level of 1 μs), was implemented. The new detector was a large area Silicon Drift Detector (SDD), specially designed for SIDDHARTA. within FP6 of the EU.

The trigger in SIDDHARTA was given by a system of scintillators which recognized a kaon entering the target making use of the back-to-back production mechanism of the charged kaons at DAΦNE from Φ decay:

$$\Phi \rightarrow K^+K^- \tag{1}$$

The SIDDHARTA setup contained 144 SDD chips, 1cm^2 each, placed around a cylindrical target, filled with high density cryogenic gaseous hydrogen (deuterium or helium). The target was made of kapton, 75μm thick, reinforced with an aluminium grid.

The SIDDHARTA setup was installed on DAΦNE in late summer 2008, and the period till the end of 2008 was used to debug and optimize the setup performances (degrader optimization included). The kaonic atoms measurements were done in 2009 and data analysis followed in the coming years, which produced the most precise measurement of kaonic hydrogen [1)] and measurements of kaonic helium 3 [2)] and kaonic helium 4 [3)], [4)]. Kaonic deuterium could not be measured by SIDDHARTA, since the signal/background was too small.

2.2 The SIDDHARTA-2 setup

The upgrade from SIDDHARTA to SIDDHARTA-2 is based on the following essential modifications:

- *Trigger geometry and target density*: By placing the upper kaon-trigger detector in front of the target entrance window the probability that a triggered kaon really enters the gas and is stopped there is optimized. Making the detector smaller than the entry area gives away some signal, but suppresses efficiently the kaonic lines from "wall-stops" (kaons entering the gas volume, but passing from the inside of the target to the cylindrical walls). The number "signal per trigger" goes up, which also reduces the accidental background coming along with every trigger.

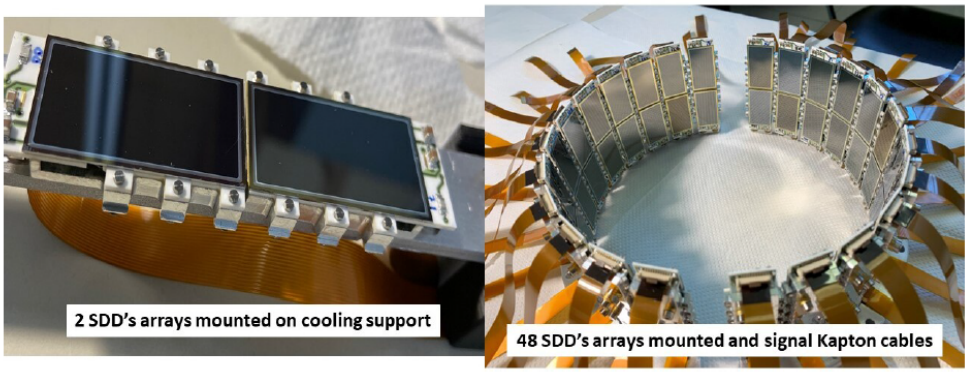

Figure 1: *Left: The two SDD arrays mounted on the cooling holder. Right: All 48 SDD arrays mounted around the target.*

- *Active shielding*: The scintillators surrounding the target are used in prompt anti-coincidence if the spatial correlation of SDD and scintillator hits indicates that it originated from a pion ("charged particle veto"). An anticoincidence covering the SDD time window of about 600 ns (with the exception of the 4 ns of the gas stopping time) reduces the accidental background. Although the scintillators have low efficiency for gammas, the abundance of secondaries from the electromagnetic showers allows a relevant reduction of accidental ("beam") background. The upper trigger scintillator has 2 functions, it is also used as an anticoincidence counter: after the kaon and eventual prompt kaon-absorption secondaries pass, it vetos beam background.

- *New SDD detectors*, produced by FBK, having a much better active/total surface ratio (about 85%, with respect to 40% in SIDDHARTA SDDs) (see Fig. 1).

- *Operating SDDs at a lower temperature*: tests indicate that an improvement of the timing resolution by a factor of 1.5 is feasible by more cooling. The signal enhancement by a factor 2 to 3 is due to moving the target cell closer to the IP, by changing its shape, by a better solid angle of the SDDs and by the higher gas density. In such conditions, with an integrated luminosity of 800 pb^{-1}, a precision similar to that obtained for kaonic hydrogen should be reachable.

Figure 2 shows an image of the SIDDHARTA-2 apparatus, where the main components are highlighted.

To perform both conditioning of the machine and tuning of the various components of the SIDDHARTA-2 setup, a reduced version, named SIDDHARTINO, with only 1/6 of the X-ray silicon drift detectors (SDD), was installed in 2019 in the interaction point of the DAΦNE accelerator. Due to the pandemic situation, the SIDDHARTINO run started in January 2021 and lasted until July 2021. During this period, two runs with a target cell filled with ^{4}He gas at about 1.5% and 0.8% of liquid helium density were performed to optimize various setup components, as well as to provide feedback to the machine during its commissioning phase. The choice of ^{4}He was dictated by the high yield of the kaonic helium-4 (3d→2p) transition allowing for fast tuning. The experimental outcomes of this run already represented the first important physics results of the SIDDHARTA-2 experiment, delivering the most precise measurement of the 2p level shift and width in the gaseous target [5].

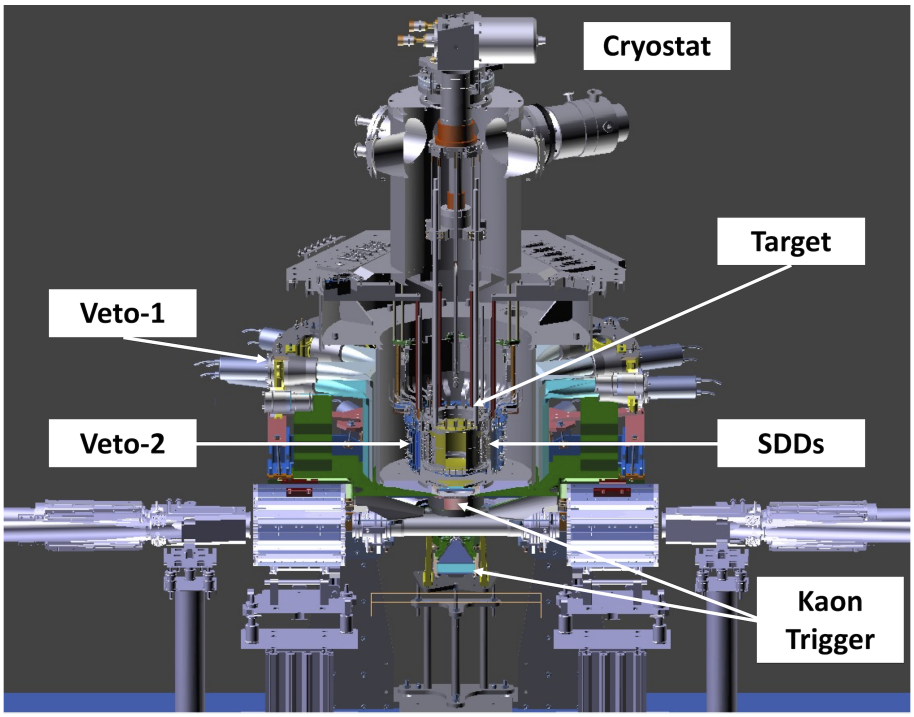

Figure 2: *Schematic view of the SIDDHARTA-2 setup.*

In the second half of 2021, the full SIDDHARTA-2 setup was installed on the DAΦNE interaction region in order to perform the difficult kaonic deuterium measurement. The optimization phase of the collider and of the full setup performance was performed, in dedicated periods, from 2021 to 2023. To optimize the performance of the detectors and of the veto systems, various measurements with helium-4 and neon gas targets were realized in this period. The kaonic deuterium data taking campaign began in May 2023 and was successfully completed in June 2024, collecting more than 800 pb^{-1} of kaonic deuterium data.

2.3 More details on 2025 SIDDHARTA-2 activities

2.3.1 Kaonic deuterium measurement

The kaonic deuterium data taking campaign began in May 2023, aiming to collect data for a total integrated luminosity of at least 800 pb^{-1} ($\sim 8\times10^7$ detected kaons), to measure the kaonic deuterium 1s level shift and width with a precision similar to that of kaonic hydrogen. The data taking was performed over four distinct runs (Table 1), with dedicated periods for the maintenance and optimization of both the experimental apparatus and the DAΦNE collider. The deuterium gas target was maintained at a temperature of approximately 26 K and a pressure of 1.30 bar, corresponding to a density of 2.28 g/l (1.4% Liquid Deuterium Density) during the first three data-taking runs. A fourth run was performed at a density of 0.8% LDD to investigate the yield as a function of density. The total integrated luminosity achieved was approximately 1 fb^{-1}, exceeding the initial experiment's requirement.

The analysis of the complete dataset is currently in progress. However, a preliminary spectrum has been extracted using data from run-1 alone. This preliminary analysis was a crucial step

	Date	Gas density [g/l]	Integrated Luminosity [pb^{-1}]
Run-1	May 2023 - July 2023	1.41% LDD	164
Run-2	October 2023 - December 2023	1.46% LDD	276
Run-3	February 2024 - April 2024	1.41% LDD	375
Run-4	May 2024 - July 2024	0.8% LDD	200

Table 1: SIDDAHRTA-2 kaonic deuterium data taking summary.

for the collaboration, for the optimization of the experimental strategy and the validation of the apparatus's performance.

Figure 3 shows the run-1 inclusive energy spectrum. The high continuous background and the fluorescence lines, due to the X-ray emission of materials placed around the SDDs, prevents the direct detection of the kaonic deuterium X-ray signal. In this context, the kaon trigger is crucial for background suppression. Events are selected based on their coincidence with a trigger signal within a 5 μs time window. The width of the time window was carefully optimized to allow for efficient signal processing and acquisition by the front-end electronics. However, charged particles from the ϕ-meson decay as well as particles originating from the beam-beam and beam gas interactions, can produce accidental trigger signals when passing through the two scintillators of the kaon trigger. These are fast Minimum Ionizing Particles (MIPs), easily distinguishable from kaons. The time difference between the signals from each scintillator and the DAΦNE radio-frequency signal divided by two is used to separate the kaon-induced triggers from those induced by MIPs, via time-of-flight analysis, with a residual MIPs contamination of less than 1%.

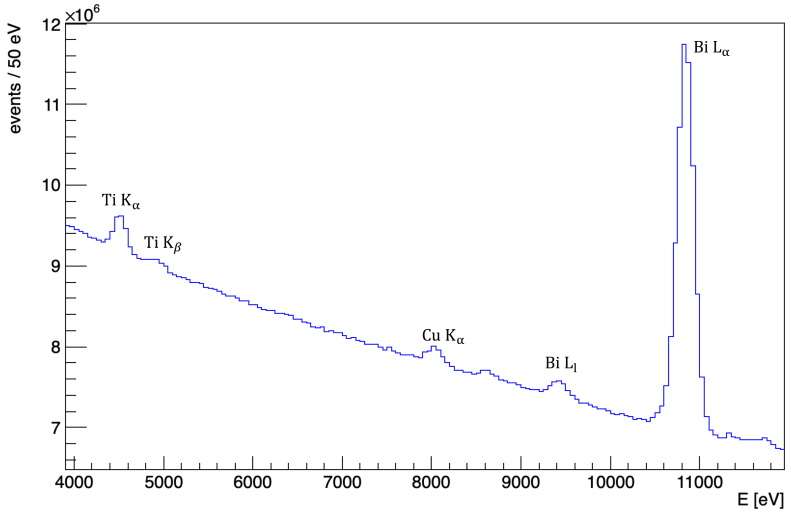

Figure 3: SIDDHARTA-2 run-1 inclusive energy spectrum.

Fig. 4-left shows, as an example, the time distribution of events measured by the two kaon trigger scintillators. It is evident that kaons arrive approximately 1.5 ns later than the MIPs. The timing information provided by the SDDs was exploited to enhance the reduction of the electromagnetic background, by selecting only X-rays within the drift time interval as shown in Fig. 4-right.

Furthermore, the implementation of veto systems contributed to an additional factor of two in

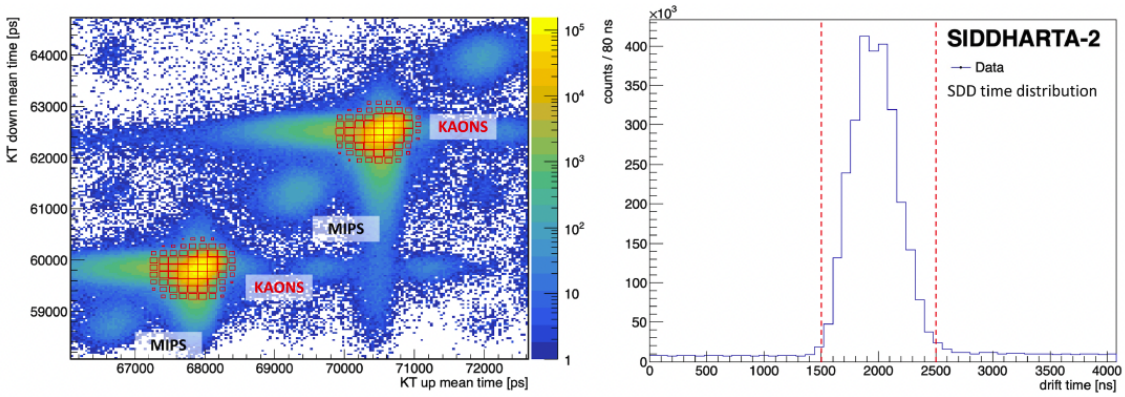

Figure 4: Left: Time distribution of the up and bottom scintillators of the kaon trigger (KT). The coincidence events related to kaons (high intensity) are clearly distinguishable from MIPs (low intensity). Right: SDDs drift time distribution, the peak corresponds to the hits on the SDDs in coincidence with the trigger, while the flat distribution is given by uncorrelated events. The dashed lines represent the acceptance window. Further details can be found in [6].

background suppression, bringing to a total background reduction of approximately 10^5, proving the remarkable performance of the SIDDHARTA-2 setup. The region of interest (ROI) for the Kα line was determined by calculating the transition energy using the Klein-Gordon equation, including vacuum polarization and recoil corrections [7]. The strong interaction shift is subtracted based on theoretical predictions summarized in Figure 5.

Assuming an energy shift between -1000 eV and -600 eV, and a width of about 1 keV, the ROI for the kaonic deuterium Kα line lies in the 6.6 - 7.4 keV energy range. In Fig. 6, a signal is visible within the defined ROI, representing a promising indication. A refined data analysis is ongoing to confirm the signal origin and to fully exploit the entire dataset.

2.4 Precision Test of Bound-State QED at Intermediate-Z with Kaonic Neon

X-ray spectroscopy of kaonic atoms has traditionally been employed to investigate the strong interaction between kaons and nuclei. However, recent advancements suggest that high-n transitions in kaonic atoms can also serve as a powerful tool for probing bound-state quantum electrodynamics (BSQED) under strong-field conditions. In particular, BSQED describes the interaction in systems where particles are electromagnetically bound to a nucleus, allowing highly accurate theoretical predictions. Traditionally, highly charged ions (HCIs) have been used for these studies [18]. However, the achievable precision is limited due to uncertainties from finite nuclear size (FNS) effects and nuclear polarization, which are larger than second-order BSQED contributions [19].

In this context exotic atoms represent a promising alternative. It has been demonstrated that muonic and antiprotonic atoms are suitable for the study of BSQED [19], and, recent measurements of kaonic neon [20] and kaonic atoms from kapton and aluminum [21] by the SIDDHARTA-2 collaboration now provide the opportunity to perform similar studies with kaonic atoms. Kaonic atoms offer a significant advantage with respect to muonic atoms due to their higher reduced mass, which enhances the sensitivity to BSQED corrections. Although antiprotonic atoms show stronger BSQED effects, their fine structure, also present in muonic atoms, requires high-resolution detectors to separate the level splittings caused by spin-orbit interactions. On the other hand, kaonic atoms do not have fine structure contributions, which simplifies both the measurement technique and the

Reference	ε_{1s} (eV)	Γ_{1s} (eV)
Kamalov *et al.* (2001)* [8]	-1080	1030
Gal (2007)* [9]	-769	674
Döring *et al.* (2011)* [10]	-779	650
Mizutani *et al.* (2013)* [11]	-887	757
Shevchenko (2012) [12]	-787	1011
Revai (2016) [13]	-800	960
Weise *et al.* (2017) [14]	-670	1016
Liu *et al.* (2020) [15]	-803	2280

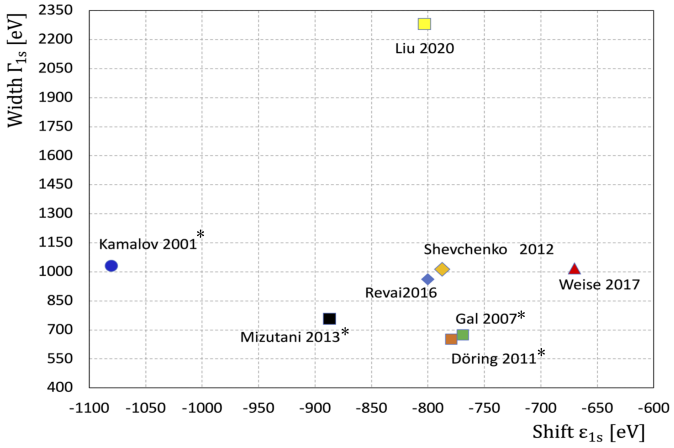

Figure 5: Comparison of kaonic deuterium 1s level shift and width predictions from various theoretical models. For the models marked with *, the energy shift and width are extracted from the scattering length using the Deser–Trueman formula [16, 17].

analysis process for extracting BSQED effects.

The SIDDHARTA-2 collaboration performed the first kaonic neon X-ray transitions measurements using a gaseous target at a density of 3.6 g/l during the 2023 SIDDHARTA-2 run at the DAΦNE collider at INFN-LNF. The kaonic neon data used for the study of BSQED corresponds to an integrated luminosity of 150 pb^{-1}, representing a 20% increase in statistics compared to our previous result [20].

To extract the transition energies from the X-ray spectrum, a maximum likelihood fit in which the observed spectral peaks were modeled using gaussian functions was performed. Each gaussian function was explicitly parameterized by the SDDs resolution, incorporating both the Fano factor and electronic noise.

Unlike earlier analyses, this study explicitly includes the two main neon isotopes, ^{20}Ne and ^{22}Ne, modeling each transition line with separate Gaussian components constrained by their natural isotopic abundances. The contribution of ^{21}Ne and uncertainties in isotopic ratios were found to be negligible. Systematic uncertainties arise mainly from energy calibration and stability over time.

Theoretical X-ray transition energies were calculated using the Multiconfiguration Dirac-Fock General Matrix Elements (MCDFGME) code (version 2025.1), developed by Desclaux and Indelicato [22, 23, 18], with the 2018 CODATA fundamental constants [24]. For each transition, the code solves the Klein-Gordon equation for the kaonic atom and including QED effects such

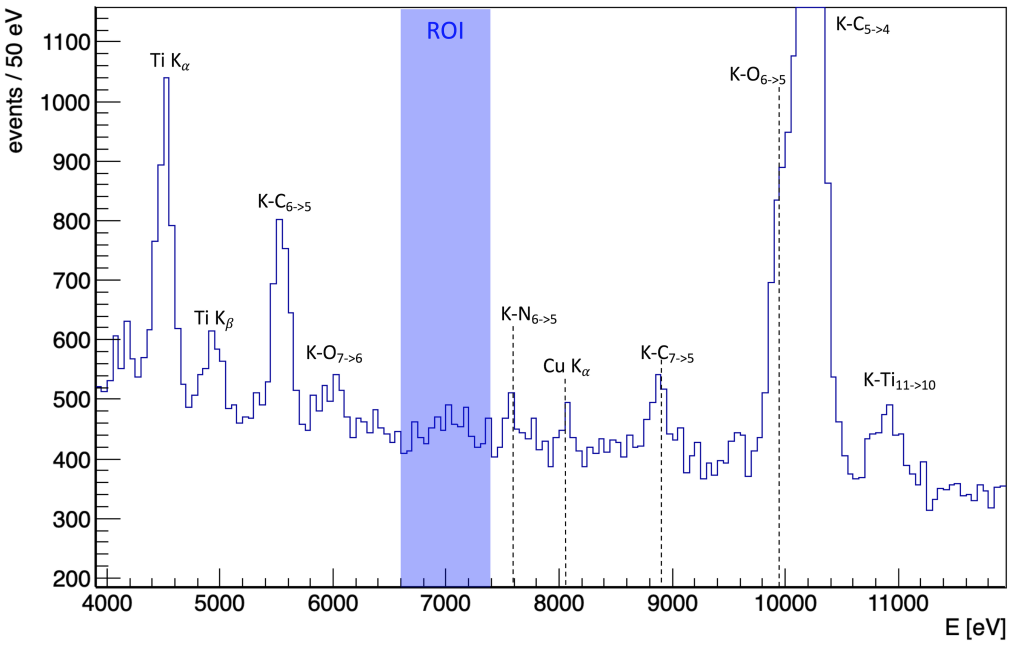

Figure 6: Preliminary SIDDHARTA-2 energy spectrum from run-1 data, after background subtraction. The region of interest (ROI) for the kaonic deuterium Kα line is highlighted.

as all-order vacuum polarization. Calculations focused on high-n circular states, neglecting finite nuclear size effects due to their minimal impact. Recoil and electron screening effects were included, and the reference kaon mass of $M_{K^-} = 493.677 MeV$ was taken from the PDG [25].

The MCDFGME calculations were also used to constrain isotopic shifts in the spectral fit. Variations of the kaon mass by ± 100 keV produced negligible changes (below 10 meV) in isotopic shifts, confirming the robustness of the modeling. Radiative and Auger transition rates were calculated using hydrogenic wavefunctions and validated against MCDFGME results, showing agreement within 1 % for high-n transitions.

The experimental KNe spectrum, shown in Fig. 7, shows three dominant peaks corresponding to the 7–6, 8–7, and 9–8 transitions, observed at approximately 9.4 keV, 6.1 keV, and 4.2 keV, respectively. In addition, several lower-intensity peaks are present which include transitions with $\Delta n > 1$, such as 10-8, 11–9, 12–9, and 12–8. The spectrum also reveals X-ray lines from other kaonic atoms formed in the setup environment, including carbon, oxygen, nitrogen, and titanium. A distinct peak at 10.8 keV is attributed to the bismuth Lα transition, originating from bismuth in the SDD ceramic materials.

The observed KNe transitions are consistent with expectations based on the competition between radiative and Auger decay channels during the cascade, as shown in Fig. 8. A qualitative analysis of the calculated rates predicts at which levels of the cascade radiative transitions begin to dominate over Auger processes. Specifically, for KNe, radiative decay becomes the dominant channel starting from an initial principal quantum number of approximately n_{init}=9 of the cascade (see Fig. 8). Transitions originating from levels below this threshold begin to appear in the spectrum, marking the progressive dominance with increasing yield of radiative emission over Auger de-excitation.

A refined fitting procedure was applied to extract the transition energies, explicitly separating

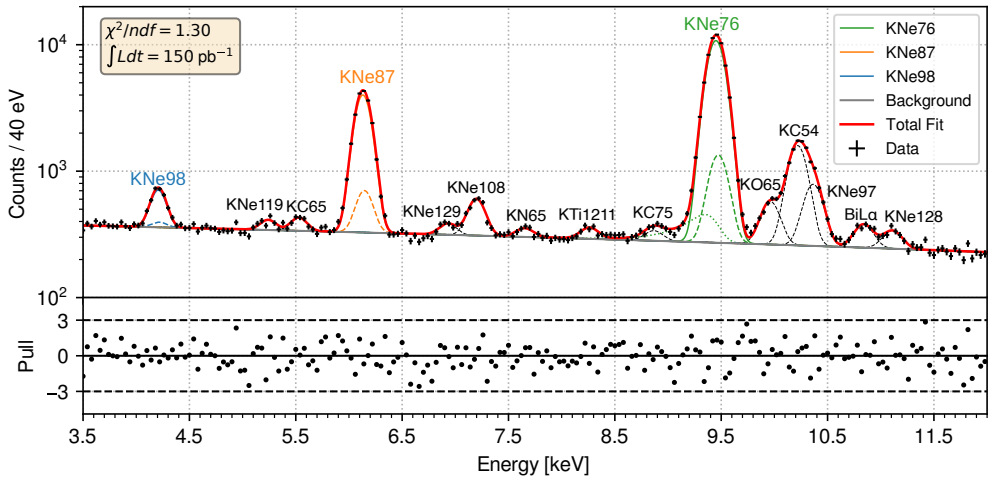

Figure 7: Fit of the KNe X-ray spectrum (top panel) in the 3.5-12 keV range, showing the counts (black), the total fit (red), individual peak contributions (dashed black), and the background (gray). The main lines of KNe are highlighted: KNe76 (green), KNe87 (orange), and KNe98 (blue), each exhibiting a double component due to the presence of two different neon isotopes (^{20}Ne and^{22}Ne). For the KNe76 peak, the tail contribution is also shown. The pull plot (bottom panel) displays the fit residuals normalized by the count errors.

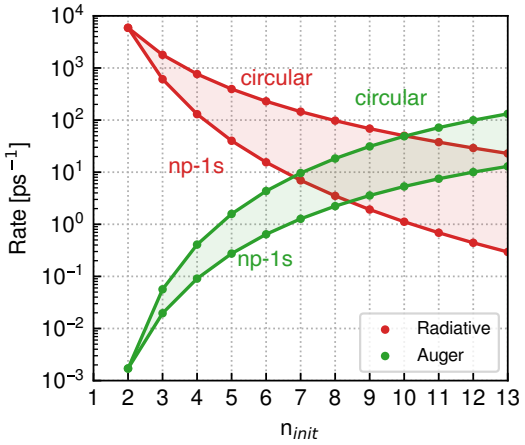

Figure 8: Radiative and Auger transition rates for KNe as a function of the initial principal quantum number n. Rates for circular ($\ell = n - 1$) and $np \to 1s$ transitions are plotted as lines, while intermediate transitions fall in the corresponding shaded regions.

Table 2: Experimental transition energies $E_{if}^{(\mathrm{exp.})}$ for KNe obtained from the fit, including statistical and systematic uncertainties, along with calculated values. All energies are given in eV.

Transition	$E_{if}^{(\mathrm{exp.})}$	$\delta E_{if}^{(\mathrm{stat.})}$	$\delta E_{if}^{(\mathrm{sys.})}$	$E_{if}^{(\mathrm{calc.})}$	$E_{if}^{(\mathrm{QED})}$	$E_{if}^{(\mathrm{QED1})}$	$E_{if}^{(\mathrm{QED2})}$	$\Delta E_{if}^{(\mathrm{isot.})}$	$\Delta E_{if}^{(\mathrm{screen.})}$	$\Delta E_{if}^{(\mathrm{PDG})}$
9l-8k	4206.97	3.43	2.00	4201.45	2.09	2.07	0.02	9.90	-0.38	0.11
8k-7i	6130.57	0.65	1.50	6130.31	5.09	5.05	0.04	14.45	-0.27	0.16
7i-6h	9450.23	0.37	1.50	9450.28	12.66	12.56	0.10	22.28	-0.18	0.24
6h-5g	15673.30	0.52	9.00	15685.39	32.75	32.51	0.24	37.01	-0.11	0.40

the contributions of the two main neon isotopes (^{20}Ne and ^{22}Ne). For the most precisely measured line, the 7–6, we find $E_{76}^{(exp.)} = 9450.23 \pm 0.37$ (stat.) $\pm$ 1.50 (syst.) eV, which is in excellent agreement with the calculated value of $E_{76}^{(calc.)} = 9450.28$ eV where the QED contribution to the transition energy is 12.66 eV.

Theoretical calculations include first- and second-order QED corrections, recoil effects, and isotopic shifts. Electron screening effects were evaluated and found to be small (below 1 eV), with only -0.18 eV for the 7–6 line. Since KNe is expected to be highly ionized when radiative transitions dominate, electron screening does not significantly affect the comparison between theory and experiment.

A broader survey of transitions up to n = 15 confirms the strong sensitivity of KNe to BSQED effects within the 2–50 keV energy range accessible to the experiment. In particular, the QED contribution to the 7–6 transition represents about 0.13% of the total transition energy—approximately an order of magnitude larger than in muonic atoms—allowing BSQED effects to be resolved with higher statistical significance. Compared to antiprotonic atoms, where finite nuclear size effects limit precision, kaonic neon offers a particularly favorable balance between enhanced QED sensitivity and controlled nuclear uncertainties, establishing it as an excellent system for precision BSQED studies.

In addition, high-n X-ray transitions offer a promising way to solve the charged kaon mass puzzle. The charged kaon mass (493.677 ± 0.013 MeV/c^2) is derived from a weighted average of six measurements [25]. A more precise determination of the kaon mass is essential for improving non-perturbative QCD calculations, including K-N scattering lengths and kaon-nucleon sigma terms, which are key to understanding chiral symmetry breaking. Improved kaon mass measurements could also reduce systematic uncertainties in the D^0 meson mass and other charmed mesons studies

The impact of the 13 keV PDG uncertainty on the charged kaon mass was investigated to assess its effect on BSQED contributions to the kaonic neon (KNe) transition energies. MCDFGME calculations were performed by varying the kaon mass, showing that transition energies depend linearly on the mass at the ppm level, while the BSQED contribution exhibits a much weaker dependence—more than two orders of magnitude smaller. The resulting theoretical uncertainties in the transition energies, propagated from the PDG kaon mass uncertainty, are reported in Table 2.

For the high-n circular transitions studied, finite nuclear size and recoil effects are negligible (few meV), and electron screening effects were evaluated separately and treated conservatively as sub-eV systematic uncertainties. The dominant theoretical uncertainty arises from the kaon mass uncertainty, leading to a 0.24 eV uncertainty for the 7–6 transition. This remains well below the experimental systematic uncertainty and more than an order of magnitude smaller than the BSQED contribution itself.

Finally, the achievable precision on the kaon mass was evaluated using the high-precision 7–6 and 8–7 transitions. Applying an iterative procedure with full propagation of statistical and systematic uncertainties, the kaon mass values and their uncertainties were extracted for each transition and for their combination, as summarized in Table 3.

Table 3: Kaon mass (M_{K^-}) extracted from different transitions, with statistical ($\delta M_{K^-}^{\text{stat.}}$) and systematic ($\delta M_{K^-}^{\text{syst.}}$) uncertainties.

Transition	M_{K^-} (MeV)	$\delta M_{K^-}^{\text{stat.}}$ (keV)	$\delta M_{K^-}^{\text{syst.}}$ (keV)
7i–6h	493.674	19	78
8k–7i	493.699	52	121
7i–6h + 8k–7i	493.677	18	66

2.5 High Purity Germanium detector for testing the feasibility study of the measurement of kaonic lead X-rays at DAΦNE for the precise determination of the charged kaon mass

A test measurement of the X-rays from kaonic lead with an HPGe detector at the DAΦNE collider was done, in order to study the feasibility of X-ray measurements from targets suitable for the determination of the charged kaon mass. This measurement was performed in parallel with SIDDHARTA-2 measurements.

High Purity Germanium detector equipped with a transistor reset preamplifier and readout with a CAEN DT5781 fast pulse digitizer was employed in the measurement of X-rays from kaonic lead.

In the SIDDHARTA-2 experiment, the target and SDD detectors of the SIDDHARTA-2 setup are placed above the Interaction Point (IP). Two plastic scintillators ($80 \times 40 \times 2$ mm^3), SC1 and SC2, which serve as a luminosity monitor in the SIDDHARTA-2 measurements, are placed on opposite sides of the IP, with the long side parallel to the beams. One Pb target of the same size as the scintillation detector SC1 and with a thickness of 1.5 mm was placed immediately behind. It was 78 mm from the IP and it completely stopped the entering kaons. The HPGe detector is a p-type detector produced by Baltic Scientific Instruments. The active part is a cylinder with a base diameter of 59.8 mm and a height of 59.3 mm. The front side of the cylinder could be positioned at a minimal distance of 155 mm from the lead target, a constraint posed by the geometry of the SIDDHARTA-2 setup. The measurement was performed at this position, which, by using GEANT4 simulations, was shown to be optimal in the given configuration. The active part of the HPGe detector was shielded by 5 cm thick lead bricks, Figure 9, right. The front brick (not shown in the figure) was 2.5 cm thick with a circular hole of 4 cm in diameter in the center, for the X-rays to reach the active part of the detector from the lead target.

The measurement was performed in parallel with the SIDDHARTA-2 experiment in June 2023. The total integrated luminosity measured with the SIDDHARTA-2 luminosity monitor was 39.4 pb^{-1}. The calibration of the energy scale of the digitizer was done by using a 1 μCi ^{133}Ba source. This was also used to determine and monitor the energy resolution of the detector during the whole period of the measurement.

Fig. 10 shows the final energy spectrum seen by the HPGe detector after applying all the cuts. Clear peaks are visible at 208.92 ± 0.17 keV, 292.47 ± 0.17 keV and 427.07 ± 0.24 keV which come from the $(10 \rightarrow 9)$, $(9 \rightarrow 8)$ and $(8 \rightarrow 7)$ transitions in the kaonic lead, respectively.

The peak at 154.2 ± 1.2 keV, from the $(11 \rightarrow 10)$ transition, is less pronounced. Besides the peak at 511 keV from positron annihilation, there are peaks which originate from the transitions in ordinary lead with which the sensitive part of the HPGe detector was shielded. Expected peaks are at 72.80 keV and 74.96 keV, which are not resolved due to the resolution of the detector, and the peak at 84.94 keV. There are also visible peaks at 356.0 keV and 81.0 keV which are due to the ^{133}Ba source, which was in front of the sensitive part of the HPGe detector during the measurement. The inset of Fig. 10 shows the peak at 292.47 ± 0.17 keV from $(9 \rightarrow 8)$ transitions in kaonic lead. The energy resolution is 3.97 ± 0.49 keV. Compared with the resolution of $4.39 \pm$

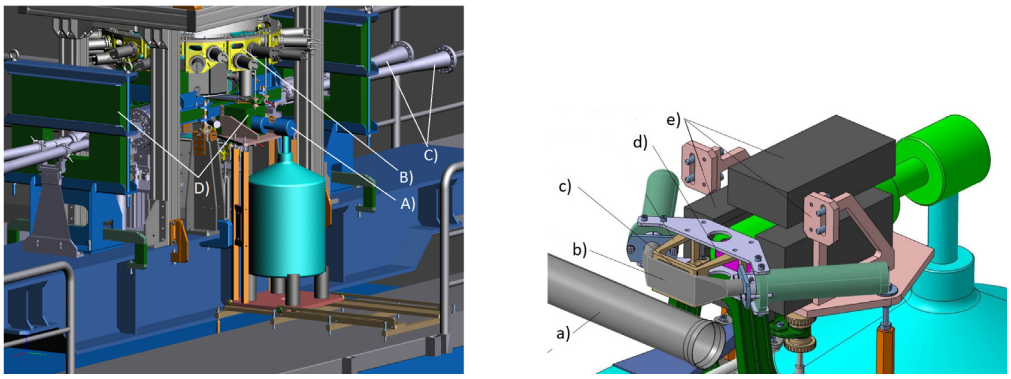

Figure 9: The location of the HPGe detector in the SIDDHARTA-2 setup, left: A) the HPGe detector, B) the SIDDHARTA-2 setup, C) beam pipes, D) shielding. Details of the HPGe setup, right: a) beam pipe, b) scintillation detector SC1, c) lead target, d) active part of the HPGe detector, e) lead shielding with holder (reported from [26]).

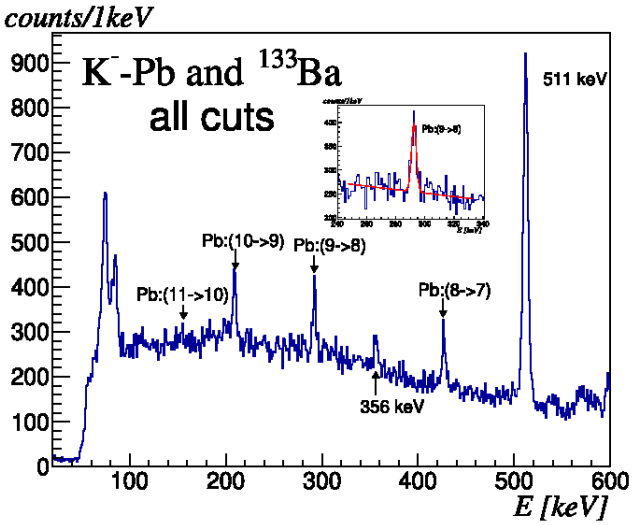

Figure 10: The spectrum seen by the HPGe detector after applying all cuts. The inset shows the peak at 292.47 ± 0.17 keV with a fit done by a Gaussian and a linear function for the background, the energy resolution is 3.97 ± 0.49 keV (FWHM) (reported from [26]).

0.02 keV at 302.9 keV of ^{133}Ba in the measurement with the beams off, it can be concluded that there is no worsening of the resolution in measurements in the full beam conditions at DAΦNE.

Assuming the standard resolution of the HPGe detector, we estimated the required number of events in the (9→ 8) transition peak to reach the 10 keV accuracy on the charged kaon mass. In a simple approach, we used the Rydberg formula for kaonic lead atoms, with the kaon-nucleus reduced mass, to obtain the relation between the precision of the transition and the accuracy of the charged kaon mass. To reach the 10 keV accuracy, the required precision of the (9 → 8) transition needs to be approximately 6 eV. Approximately 8500 events in the (9 → 8) transition peak are needed to reach the 10 keV accuracy on the charged kaon mass, assuming a detector with a resolution of 1.3 keV at 292 keV. The total number of events in the (9 → 8) peak in our measurement is 770 ± 65. This implies that a total integrated luminosity of 435 pb^{-1} is needed to achieve the required accuracy by using only the (9 → 8) transition in kaonic lead. This measurement serves as a test bed for future dedicated kaonic X-rays measurements for the more precise determination of the charged kaon mass.

2.6 Characterization for CZT Detection System in a collider environment

SIDDHARTA2 collaboration has developed a new detection system based on the appealing CZT compound semiconductor in order to measure the strong interaction in kaonic atoms systems in the intermediate-mass range (Al, F, C, S). The transitions of interest for such systems lay in the 30-300 keV range, where CZT devices are the radiation detectors best fulfilling the high efficiency and high-resolution requirements demanded to measure the emitted X-rays with precisions of a few tens of eV, thus pinning down those of the older experiments.

Moreover, with their excellent performances at room temperatures, CZT detectors allow for realizing small and compact detection systems, easy and fast to be installed and integrated with the existing SIDDHARTA-2 apparatus. The arrangement of this detection system was particularly challenging because this is the first application in a collider and this experiment can open the way to new use in this environment.

The CZT detection system consists of eight single 13 mm × 15 mm × 5 mm quasi-hemispherical CZT detectors enclosed in a thin aluminum box with an 0.27 μm thick aluminum window. To stabilize the temperature of the electronic components (not of the crystals), a FRYKA DLK 402 recirculating chiller working at a temperature of 15 ° C, was put on the lower side of the aluminum box. The front part of the aluminum box was enclosed with a lead shielding to lower down the intense radiative background caused by the particle losses at the last focusing quadrupole near the interaction point at DAΦNE that cause a huge background for kaonic atoms researches, being the detector as close as possible to the interaction point.

The detector was placed at 25 cm far from the IP of the DAΦNE collider, and between them, 10.2 cm from the IP, a plastic scintillator read by two PMTs was placed, working as a luminosity monitor for the whole experiment (LUMI). Immediately after the LUMI, a solid target was placed, in which the kaons stopped and formed atomic states with the nuclei of the target material. In the beginning of the run, an aluminum target was used. Finally, the X-rays emitted by the kaonic atoms were detected by the CZT system. The detectors were positioned 17 cm from the target. A schematic view of the setup is shown in Figure 11.

During the data taking of the SIDDHARTA-2 experiment, the CZT detector collected data for several months. At first the detector experienced a long phase of optimization of the setup, the HV, and the detector's position. The calibrations with source (^{152}Eu) was done and has been thoroughly described in a previous work [28].
The detector calibrated with this method demonstrated good energy stability across the entire data-taking period, confirming the reliability of the system and its resistance to potential issues arising from electronics or environmental conditions.

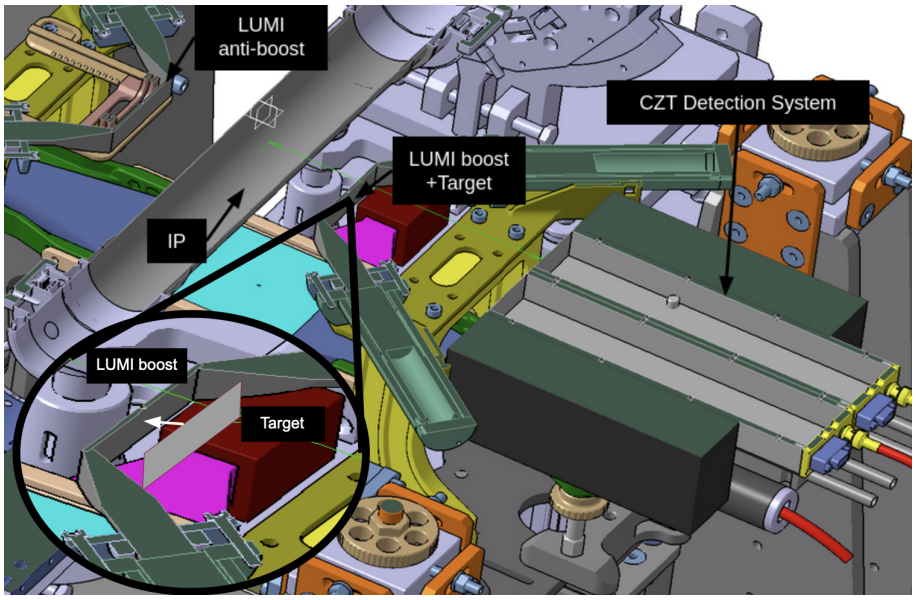

Figure 11: Schematic view of the experimental setup of the CZT detection system in DAΦNE. A description of the materials follows: The DAΦNE beam pipe (around the IP in the Figure, displayed in grey) is made by a mixture of aluminum and carbon fiber; the LUMI detectors (housing and lightguides shown wrapped in aluminized mylar, coloured in silver); the Target (shown in light gray) is an aluminum plate; the CZT detection system's box (displayed in light grey) is made of aluminum; mechanical supports and mounting structures (brackets yellow, kinematic mounts orange) are made of aluminum alloy. Additional small components visible: an electronics/power module (magenta) and support plates (cyan/turquoise).

The first linearity and stability characterization for CZT detection system in a collider was done, by performing a run with a source and the collider beam on, with the source placed in front of the detection system. The results of the tests are:

- The study on the short-term stability of the detectors showed that the outcome signals of the complex apparatus do not depend on environmental conditions, confirming the perfect stability of these kinds of detectors also after being exposed at high rates.
- The study of the long-term stability showed that the system is extremely stable also after switching off the apparatus and the machine and after changing some detectors, confirming the robustness of the electronics and the hardware and software data acquisition.
- The single long calibration every two of three weeks, even a month, is sufficient to control accurately the systematics and to obtain precise results on the kaonic atoms observables.
- The high rate due to the environment does not affect at all the detector properties.

One of the primary challenges for this detector is the suppression of intense background radiation, typical of collider environments. In this context, the signals from the two LUMI scintillators, combined with the DAΦNE collider radiofrequency (RF) signal, can be used to discriminate charged kaon pairs originating from the interaction point [29, 30]. The narrow momentum spread and low β of the kaons from ϕ meson decays allow for the selection of kaon-related signals through

time-of-flight measurements. The TAC-processed luminometer used in the experiment was shown to effectively distinguish between kaons and minimum ionizing particles (MIPs) [29, 30]. For the 2024 run, the combined signal from both the boost side and antiboost side LUMIs was employed, representing a significant improvement in kaon pair discrimination capability. Figure 12 shows the spectrum of the two luminometer signals after TAC processing and their combined 2D histograms. The narrower peaks correspond to the kaon windows, due to the smaller momentum spread compared to MIPs. Four similar patterns, corresponding to kaon and MIP arrivals, appear because the TAC operates at a frequency of 1/4 of the DAΦNE RF, which is 3.7 MHz [31]. The final selection applied to TAC1 and TAC2 for one of the four patterns is shown in Figure 12-right. The green box indicates the optimized region corresponding to the maximum signal significance.

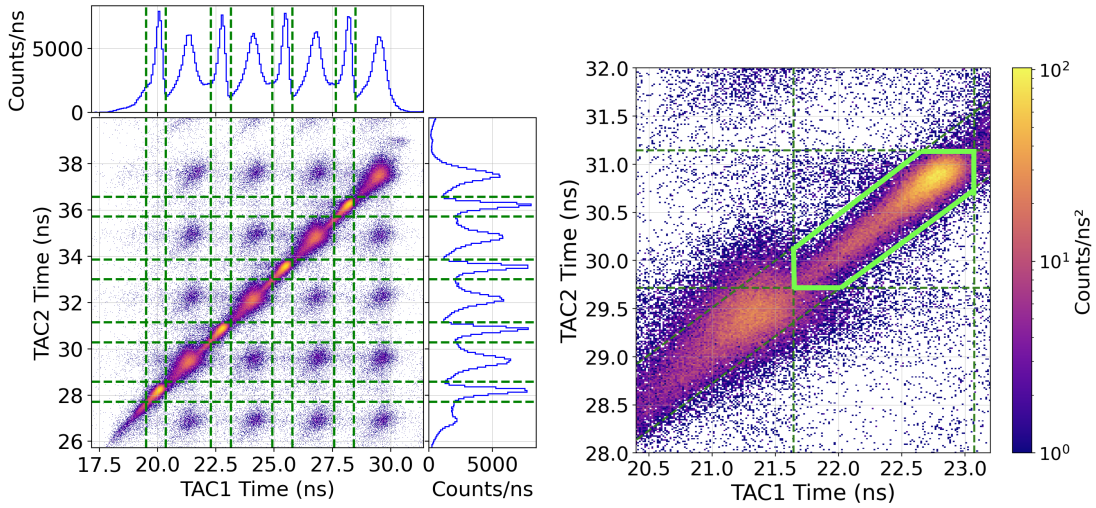

Figure 12: Left: 2D histogram of TAC1 vs TAC2. Kaon-related coincidences appear as narrow peaks within the green guidelines. Right: 2D histogram of the two TAC signals from the LUMI scintillators for one kaon-MIP couple, with the optimized selection guidelines shown as dotted green lines. The selected kaon windows correspond to the hexagonal areas formed by the broader rectangles along the diagonal, combined with the region inside the diagonal cuts. These selected area is highlighted in light green in the figure.

The time distribution of detector signals is essential for applying time-based selection cuts. A clear time correlation exists between kaon production and detector signals, appearing as a peak in the distribution of the time difference (Δt) between the trigger and the detector event. By selecting events within this peak region, background from uncorrelated processes can be significantly reduced, improving the overall signal quality. The optimized kaon time window is shown in the Figure 13, and the main contribution to the width of the Δt distribution comes from the charge drift time in the CZT detector.
A $\approx$ 100 ns Δt window gives a very good result, compared to that achieved with the SDDs used in the experiment [(507.60 $\pm$ 0.47) ns at FWHM] [32].

After applying the two selection steps, about 95% of the triggered events are rejected. A previous study evaluated the overall rejection factor using the coincidence of a kaon signal in a single LUMI scintillator combined with a variable Δt time window. Within a 100 ns Δt window, a rejection factor of about 10^6 was achieved relative to the total number of triggered and untriggered events. A similar rejection efficiency is expected when considering all detector events. These results

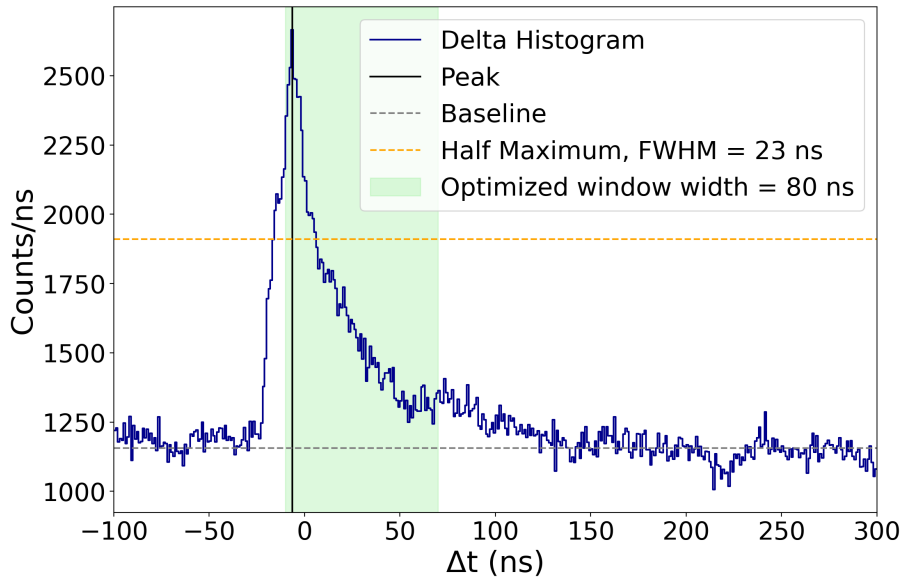

Figure 13: Measured cumulative spectrum of the drift time with the optimized limits of the signal region reported in green. In the legend the FWHM of the peak and the width of the selected window are reported.

demonstrate the method's strong background suppression capability and its suitability for future precision measurements in high-radiation environments.
The fitted spectrum with kaon and Δt selections, acquired by the CZT detection system is reported in Figure 14, together with the residuals.
The resulting energy spectrum, after applying all selection criteria, clearly shows the first observed kaonic-aluminum transition peaks using a room-temperature detector. For the 5-4 transition at 50 keV, 362 ± 41 (stat.) ± 20 (sys.) signal events were observed over 1698 ± 197 (stat.) ± 25 (sys.) background events within $\pm 5\sigma$, with an energy resolution of 9.2% FWHM. For the 4-3 transition at 106 keV, 295 ± 50 (stat.) ± 20 (sys.) signal events were measured over 2939 ± 500 (stat.) ± 16 (sys.) background events, with an energy resolution of 6.6% FWHM.

These results demonstrate both the effectiveness of the CZT-based detection system developed by the SIDDHARTA-2 collaboration and the feasibility of precision kaonic atom spectroscopy with CZT detectors. This study paves the way for new applications of CZT detectors in kaonic-atom spectroscopy, both at DAΦNE and at J-PARC, demonstrating their strong potential for precision measurements in challenging experimental environments.

2.7 New 1mm thick Silicon Drift Detectors for future research of Kaonic Atoms

Looking beyond the current measurements, the collaboration is developing EXKALIBUR [33], an extension of the SIDDHARTA-2 experiment aimed at exploring kaonic atoms with heavier nuclei, such as lithium, beryllium, and neon. These systems emit X-rays at higher energies, requiring detectors with enhanced stopping power and efficiency in the 10–30 keV range. To meet this need, new 1 mm-thick monolithic SDD arrays are being developed in collaboration with Politecnico di Milano (PoliMi) and Fondazione Bruno Kessler (FBK) [34]. Compared to the 450 µm devices currently used, these new sensors significantly increase the detection efficiency for high-energy X-rays while preserving excellent energy resolution and timing performance. To achieve this, the new

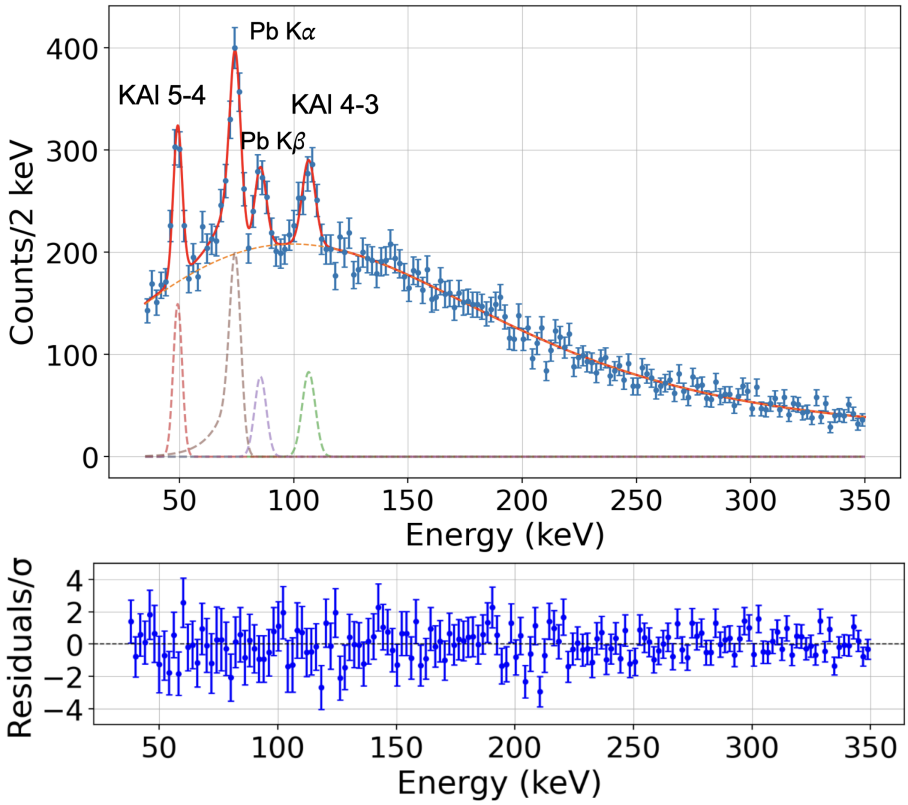

Figure 14: Fit to the data after the optimized selection (up). The errors of the number of counts reported are the statistical errors ($1/\sqrt{counts}$). The plot of residuals for each bin normalized at their standard deviation (σ) is also reported (down).

sensors are fabricated on 1 mm-thick silicon substrates, compared to the 450 µm of the current devices. This modification increases the detection efficiency by approximately 70% and 100% for 20 keV and 30 keV X-rays, respectively and will make possible to observe transitions in kaonic lithium and beryllium, like those listed in Table 4, all lying in the 10–30 keV range.

A prototype of the new array is shown in Figure 15. The geometry of the active area has been maintained identical to that of the previous design, consisting of a 2×4 array of square pixels with an 8 mm pitch, for a total active area of 32×16 mm^2. However, to ensure optimal charge collection in the thicker material, the termination structures around the drift rings have been partially redesigned. The width of the outer drift ring and the number of external floating guard rings were increased to better control the lateral depletion and improve charge collection efficiency within the nominal active region. These modifications led to a slightly larger inactive border, bringing the total chip size to 36×20 mm^2.

In Table 5 are reported some of the key features of the new SDDs in comparison to the 450 µm ones.

The first prototypes of these 1 mm SDD arrays are currently under bias voltage characterization at INFN-LNF. These tests aim to optimize the spectroscopic performance – in terms of linearity and energy resolution – of the detector by finding the best operating conditions, verify time resolution, and assess the overall performance in view of their integration into the

Lithium-6		Lithium-7		Beryllium-7	
Transition	Energy [keV]	Transition	Energy [keV]	Transition	Energy [keV]
$3 \rightarrow 2$	15.085	$3 \rightarrow 2$	15.261	$3 \rightarrow 2$	27.560
$4 \rightarrow 2$	20.365	$4 \rightarrow 2$	20.603	$4 \rightarrow 3$	9.646
$5 \rightarrow 2$	22.809	$5 \rightarrow 2$	23.075	$5 \rightarrow 3$	14.111

Table 4: Main X-ray transition energies for kaonic lithium and beryllium atoms targeted by EXKALIBUR. The energy range of 15–30 keV is well covered by the 1 mm SDDs.

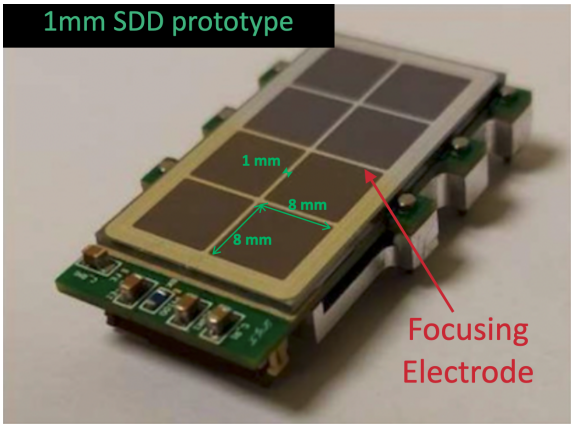

Figure 15: Prototype of the new 1 mm SDD array developed in collaboration with FBK.

SIDDHARTA-2. In Figure 16 is presented an energy spectrum acquired from the newly developed 1 mm SDDs. Distinct peaks corresponding to characteristic X-ray lines up to about 30 keV are observed, confirming the detector's capability to efficiently measure photons in the energy region relevant for heavier kaonic atom transitions.

These results confirm the suitability of the new devices for extending the SIDDHARTA-2 measurement range and improving the sensitivity of future experiments to the kaon–nucleus interaction. Future work will focus on full characterization of the detectors under operating conditions and their integration into the SIDDHARTA-2 [6]. Once implemented, the upgraded system will open the way to a new generation of precision measurements on kaonic atoms, providing valuable insights into the low-energy behavior of the strong interaction in the strangeness sector.

	450 µm	1 mm
QE@20 keV	34 %	60 %
QE@30 keV	10 %	24 %
FWHM@6.4 keV	∼160 eV	∼150 eV
Total chip size	34×18 mm^2	36×20 mm^2
Active area	32×16 mm^2	32×16 mm^2
Focusing Electrode	No	Yes

Table 5: Comparison of the main characteristics of the previously used 450 µm-thick SDDs and the new 1 mm-thick devices, including quantum efficiency at different energies, energy resolution at 6.4 keV (reference point), geometrical dimensions, and electrode configuration.

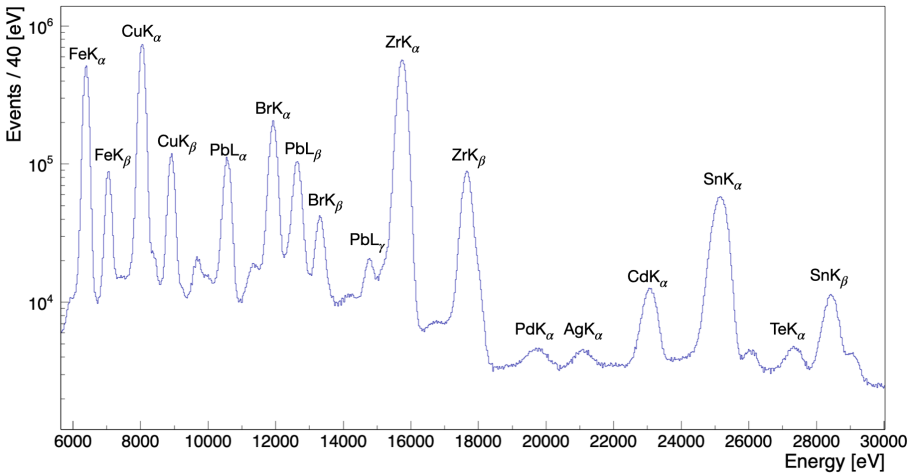

Figure 16: X-ray energy spectrum acquired with the 1 mm SDD prototypes, shown with a bin width of 40 eV. Characteristic lines from various calibration (Fe, Cu, Br, Zr, Sn) and contamination (Pb, Pd, Ag, Cd, Te) sources are clearly visible in the 6–30 keV energy range.

2.8 Plan for the SIDDHARTA-2 activities in 2026

The LNF group main activities in SIDDHARTA-2 for 2026 will be the following ones:

- refined data analysis using also Machine Learning techniques to extract the shift and width of kaonic deuterium transitions to fundamental level
- analyses of post-calibration kaonic atoms data (with various solid targets)
- data analysis of the test run with CdZnTe detectors, which are ideal for detecting transitions toward both the upper and lower levels of intermediate-mass kaonic atoms, like kaonic carbon and aluminium
- consolidation of the proposal for kaonic atoms measurements beyond SIDDHARTA-2, i.e. EXKALIBUR program
- test of the new Silicon Drift Detectors 1mm thick, developed in collaboration with Fondazione Bruno Kessler.

3 Events organization in 2025

In 2025 the following event related to the physics of SIDDHARTA-2, was organized:

- Workshop on Fundamental Physics with Exotic Atoms, 23–25 June 2025, Frascati, Italy. https://agenda.infn.it/event/46674/
- High Precision X-ray Measurements 2025, 16-20 July 2025, Frascati, Italy. https://agenda.infn.it/event/43727/

Acknowledgements

The support from LNF Directors, Dr.ssa Paola Gianotti, and the DAΦNE and BTF-LNF teams are gratefully acknowledged.

4 List of Conference Talks by LNF Authors in 2025

1. F. Artibani, "Novel Solid State CZT Detectors for Fundamental Physics", Workshop on Fundamental Physics with Exotic Atoms, 23–25 June 2025, Frascati, Italy.
2. F. Artibani, "Novel CZT Detectors for kaonic atoms spectroscopy", High Precision X-ray Measurement – HPXM2025, 16–20 June 2025, Frascati, Italy.
3. F. Artibani, "Novel CZT Detectors for kaonic atoms spectroscopy", 111° Congresso della Società Italiana di Fisica, 22–26 September 2025, Palermo, Italy.
4. F. Artibani, "Intermediate-mass Kaonic Atoms Measurements with Novel CZT Detector" (poster), XIII International Conference on Kaon Physics – KAON2025, 8–12 September 2025, Mainz, Germany.
5. F. Artibani, "Novel CZT Detectors for kaonic atoms spectroscopy", Exotic atoms: fundamental aspects, applications and advances in radiation detectors, 3–5 December 2025, Zagreb, Croatia.
6. P. Barcella, "Test with Synchrotron Light of ASCANIO: an Innovative Backscattering Geometry Spectrometer", IEEE NSS-MIC Conference, 1-8 November 2025, Yokohama, Japan.
7. G. Borghi, "Silicon Drift Detectors and Related Electronics for Fundamental Physics and Synchrotron Applications", 2nd Workshop on Silicon Sensors, 12-14 August 2025, Berg, Germany.
8. C. Curceanu, "A Strangeness Odyssey: Kaonic Atom Measurements at the DAΦNE Collider" 61st International Winter Meeting on Nuclear Physics 27-31 January 2025, Bormio, Italy.
9. C. Curceanu, "Kaonic atoms From DAΦNEto J-PARC", International Workshop and Town Meeting on the Extension Project for the J-PARC Hadron Experimental Facility (HEF-ex WS/Town-Meeting 2025).
10. C. Curceanu, "Strangeness in all its forms: reflections and perspectives from HYP2025", The 15th International Conference on Hypernuclear and Strange Particle Physics (HYP2025), 29 September - 3 October 2025, Tokyo, Japan.
11. C. Curceanu, "Strange Exotic Atoms: precision frontiers in fundamental interaction studies", Workshop Exotic Atoms: Fundamental aspects, applications and advances in radiation detectors, 3-5 December 2025, Zagreb, Croatia.
12. F. Clozza, "Precision X-Ray measurements with Silicon Drift Detectors in the SIDDHARTA-2 experiment", High Precision X-ray Measurements 2025, 16-20 July 2025, Frascati, Italy.
13. F. Clozza, "Silicon Drift Detectors for the new generation of Kaonic Atoms measurements", Workshop on Fundamental Physics with Exotic Atoms 2025, 23-15 July 2025, Frascati, Italy.
14. F. Clozza, "High-Precision Kaonic Atom Measurements with SIDDHARTA-2 at the DAΦNE Collider" (poster), XII International Conference on Kaon Physics KAON25, 8-12 September 2025, Mainz, Germany.

15. F. Clozza, "High-precision kaonic atom measurements with SIDDHARTA-2 at the DAΦNE collider", SIF 111 - Congresso Nazionale, 22-26 September 2025, Palermo, Italy.

16. F. Clozza, "Kaonic Hydrogen isotopes for unique strong interaction studies", Exotic atoms: fundamental aspects, applications and advances in radiation detectors, 3-5 December 2025, Zagreb, Croatia.

17. S. Manti, "Kaonic Neon Spectroscopy: Testing Bound-State QED, Extracting the Kaon Mass and Probing Beyond Standard Model Physics", Workshop on Fundamental Physics with Exotic Atoms, 23-25 June 2025, Frascati, Italy.

18. S. Manti, "High-Precision Spectroscopy of Kaonic Atoms at SIDDHARTA-2: probing fundamental interactions", Workshop on Standard Model and Beyond 2025, Mon Repos, 24-29 August 2025, Corfu, Greece.

19. S. Manti, "High Precision X-ray Spectroscopy: from Kaonic Atoms to Societal Applications", 2nd Symposium on new trends in nuclear and medical physics, 24-26 September 2025, Krakow, Poland.

20. S. Manti, "Testing Bound State QED in Strong Fields with Kaonic Atoms", Exotic atoms: fundamental aspects, applications and advances in radiation detectors, 3-5 December 2025, Zagreb, Croatia.

21. B. Pedretti, "Real-Time Active Collimation of Charge-Sharing Events in Monolithic SDD Arrays", IEEE NSS-MIC Conference, 1-8 November 2025, Yokohama, Japan.

22. B. Pedretti, "High-Density Monolithic SDD Arrays for High-throughput X-Ray Spectroscopy Applications", IEEE NSS-MIC Conference, 1-8 November 2025, Yokohama, Japan.

23. F. Sgaramella, "Probing Fundamental Interactions with Kaonic Atom X-ray Spectroscopy: From strong-field QED to low-energy QCD", HPXM-2025, 16-20 June 2025, Frascati, Italy.

24. F. Sgaramella, "Kaonic Atoms X-ray Spectroscopy with SIDDHARTA-2: The First Measurement of Kaonic Deuterium", Fundamental Physics with Exotic Atoms, 23-25 June 2025, Frascati, Italy.

25. F. Sgaramella, "Exploring the Strangeness Frontiers: Kaonic atoms X-ray spectroscopy at DAΦNE with SIDDHARTA-2", HYP-2025, 29 Sep. – 3 Oct. 2025, Tokyo, Japan.

26. A. Scordo, "Kaonic Atoms measurements with the SIDDHARTA-2 experiment at DAΦNE", invited plenary talk at the "HADRON2025" conference, 27-31 March 2025, Toyonaka Campus, Osaka University, Japan.

27. A. Scordo, "The quest for kaonic atoms' measurements: technological challenges and future perspectives", invited talk at YITP international workshop on Hadron in Nucleus (HIN2025) 2-4 April 2025, Yukawa Institute for Theoretical Physics, Kyoto University, Japan.

28. A. Scordo, "X-ray Spectroscopy of Kaonic Atoms with CdZnTe Quasi-Hemispherical Detectors", talk at the "IEEE-MIC-NSS-RTSD 2025" conference, 1–8 NOVEMBER 2025, YOKOHAMA, Japan.

29. A. Scordo, "Cutting-edge X-ray detectors for precision spectroscopy of exotic atoms", invited Talk at the "Exotic atoms: fundamental aspects, applications and advances in radiation detectors" workshop, 3-5 December 2025, Zagreb, Croatia.

30. F. Sirghi, "Overview of Technological Challenges in Exotic Atom Precision Experiments", Workshop on Fundamental Physics with Exotic Atoms, 23-25 June 2025, LNF-INFN, Frascati, Italy.

31. D. Sirghi, "The physics of kaonic physics in the last 25 years, Workshop on Fundamental Physics with Exotic Atoms, 23-25 June 2025, LNF-INFN, Frascati, Italy.

32. D. Sirghi, "The physics of kaonic physics in the last 25 years", Workshop "Exotic atoms: fundamental aspects, applications and advances in radiation detectors", 3-5 December 2025, Zagreb, Croatia.

5 Publications in 2025

1. S. Manti, A. Clozza, G. Moskal, K. Piscicchia, D. Sirghi, F. Sirghi, C. Curceanu and A. Scordo, Recent Developments of the VOXES Von Hamos X-ray Spectrometer for Laboratory XES and XAS Studies, [arXiv:2512.03826 [physics.app-ph]].

2. F. Clozza, F. Sgaramella, L. Abbene, F. Artibani, M. Bazzi, G. Borghi, D. Bosnar, M. Bragadireanu, A. Buttacavoli and M. Carminati, *et al.* New 1mm thick Silicon Drift Detectors for future researches of Kaonic Atoms and the Pauli Exclusion principle, [arXiv:2512.02613 [physics.ins-det]].

3. F. Artibani, L. Abbene, A. Buttacavoli, M. Bettelli, G. Gerardi, F. Principato, A. Zappettini, M. Bazzi, G. Borghi and D. Bosnar, *et al.* CZT Detectors for kaonic atoms spectroscopy, [arXiv:2512.02599 [physics.ins-det]].

4. F. Artibani, L. Abbene, A. Buttacavoli, M. Bettelli, G. Gerardi, F. Principato, A. Zappettini, M. Bazzi, G. Borghi and D. Bosnar, *et al.* Time-based selection of kaonic atom x-ray events with quasi-hemispherical CZT detectors at the DAΦNE collider, Measur. Sci. Tech. **37** (2026) no.3, 035108 doi:10.1088/1361-6501/ae3203 [arXiv:2511.02671 [physics.ins-det]].

5. L. Abbene, A. Buttacavoli, F. Principato, G. Gerardi, M. Bettelli, A. Zappettini, F. Artibani, A. Clozza, F. Sgaramella and F. Sirghi, *et al.* X-Ray Spectroscopy of Kaonic Atoms With Cdznte Quasi-Hemispherical Detectors, doi:10.1109/NSS/MIC/RTSD57106.2025.11287668

6. F. Artibani, F. Clozza, L. Abbene, M. Bazzi, G. Borghi, D. Bosnar, M. Bragadireanu, A. Buttacavoli, M. Cargnelli and M. Carminati, *et al.* Low-Energy Kaon-Nuclei Interaction studies at the DAΦNE Collider: a Strangeness Odyssey, PoS **QCHSC24** (2025), 266 doi:10.22323/1.483.0266

7. S. Manti, L. Abbene, F. Artibani, M. Bazzi, G. Borghi, D. Bosnar, M. Bragadireanu, A. Buttacavoli, M. Carminati and A. Clozza, *et al.* EXKALIBUR: Towards a Kaonic Atoms Periodic Table to test Fundamental Interactions, [arXiv:2510.21519 [nucl-ex]].

8. T. Akaishi, H. Asano, X. Chen, A. Clozza, C. Curceanu, R. Del Grande, C. D. Han, T. Hashimoto, M. Iliescu and K. Inoue, *et al.* Measurement of 3,4He(K−,π0)Λ3,4H reaction cross section and evaluation of hypertriton Λ binding energy, Phys. Lett. B **873** (2026), 140163 doi:10.1016/j.physletb.2026.140163 [arXiv:2509.16967 [nucl-ex]].

9. S. Manti *et al.* [SIDDHARTA-2], Precision Test of Bound-State QED at Intermediate-Z with Kaonic Neon, [arXiv:2508.08161 [physics.atom-ph]].

10. F. Artibani *et al.* [SIDDHARTA-2], Tests of New CZT detectors at DAΦNE collider for Kaonic Atoms Measurements, PoS **DISCRETE2024** (2025), 031 doi:10.22323/1.481.0031

11. A. Scordo *et al.* [SIDDHARTA-2], Kaonic atoms studies with the SIDDHARTA-2 experiment, PoS **QNP2024** (2025), 205 doi:10.22323/1.465.0205

12. F. Sakuma *et al.* [J-PARC E80], Light Kaonic Nuclei at J-PARC, PoS **QNP2024** (2025), 211 doi:10.22323/1.465.0211

References

1. M. Bazzi *et al*, Phys. Lett. B **704** , 113 (2011).
2. M. Bazzi *et al*, Phys. Lett. B **697** , 199 (2011).
3. M. Bazzi *et al*, Phys. Lett. B **681** , 310 (2009).
4. M. Bazzi *et al*, Phys. Lett. B **714** , 40 (2012).
5. D. Sirghi *et al*, J. Phys. G 49 (2022) 0551026.
6. F. Sirghi *et al*, JINST, **19** , number 11, P11006 (2024)
7. J.P. Santos *et al*, Phys. Rev. A **71** 032501 (2025)
8. S.S Kamalov *et al*, Nucl. Phys. A **690** 494 (2001)
9. A. Gal, Int. J. Mod. Phys. A **22** 226 (2007)
10. M. Döring, M. and U. -G Meißner, Phys. Lett. B **704** 663 (2011)
11. T. Mizutani *et al*, Phys. Rev. C **87** n.3 035201 (2013)
12. N.V. Shevchenko, Nucl. Phys. A **890-891** 50 (2012)
13. J. Revai, Phys. Rev. C **94** n.5 054001 (2016)
14. T Hoshino *et al*, Phys. Rev. C **96** n.4 045204 (2017)
15. Z.W Liu *et al*, Phys. Lett. B **808** 135652 (2020)
16. U. -G Meißner *et al*, Eur. Phys. J. C **35** 349 (2004)
17. U. -G Meißner *et al*, Eur. Phys. J. C **47** 473 (2006)
18. P. Indelicato, J. Phys. B **52** n.23 232001 (2019)
19. N. Paul *et al*, Phys. Rev. Lett. **126** n.17 173001 (2021)
20. F. Sgaramella *et al*, Phys. Lett. B **865** 139492 (2025)
21. F. Sgaramella *et al*, Eur. Phys. J. A **59** n.3 56 (2023)
22. J. V. Mallow *et al*, Physical Review A **17** n.6 1804 (1978)
23. *et al*J.P. Santos Physical Review A bf 71 n.3 032501 (2005)
24. E. Tiesinga *et al* Reviews of Modern Physics **93** n.2 025010 (2021)
25. S. Navas*et al*, Physical Review D **110** n.3 030001 (2024)
26. D. Bosnar *et al*, Nucl.Instrum. Meth. A **1069** (2024) 169966.

27. A. Scordo *et al*, Nucl.Instrum .Meth. A **1060** (2024) 169060
28. L. Abbene *et al*, Sensors **24** n.23 7562 (2024)
29. L. Abbene *et al*, Sensors **23** n.17 7328 (2023)
30. A. Scordo *et al*, Nucl. Instrum. Meth. A **1060** 169060 (2024)
31. C. Milardi *et al*, Int. J. Mod. Phys. A **24** 360 (2009)
32. F. Sgaramella *et al*, Condens. Mat. **9** n.1 16 (2024)
33. F. Artibani *et al*, PoS QCHSC **24** 266 (2025)
34. L. G. Toscano *et al*, JINST **19** P07039 (2024)